Low-Rank Dynamic MRI Imaging Model Based on MC Penalty Function

Zhijun Luo, Lirong Wang, Zhibin Zhu, and Yingying Li

***Abstract*—In the research of dynamic MRI imaging, we have utilized the minimax-concave (MC) function to replace the traditional nuclear norm, thereby significantly enhancing the model's fitting accuracy. The Total Variation (TV) duality technique is introduced to refine the model resolution further, better capturing underlying structures in MRI data. The splitting method is also employed to establish a comprehensive solution framework for the model. A high-efficiency algorithm, designed using the proximity operator, is developed to solve sub-problems within this framework, ensuring swift and accurate convergence. Numerical experiments on various dynamic MRI datasets and undersampling templates demonstrate that the new method outperforms traditional approaches in several key metrics, including CPU runtime, iteration count, and reconstruction performance. The new method reduces computational overhead, expedites the image reconstruction process, and significantly improves the quality of reconstructed images.**

***Index Terms*—DMRI reconstruction, MC function, Low-rank, Primal-dual**

I. Introduction

DYNAMIC magnetic resonance imaging (DMRI) is a revolutionary advancement in medical diagnostic technology, providing both temporal and spatial information through magnetic resonance signals. This technique has a wide range of clinical applications, particularly cardiovascular imaging [1]. However, traditional DMRI methods suffer from longer imaging times, which have several drawbacks. Firstly, longer scanning times limit the spatiotemporal resolution of MR images and result in a lower signal-to-noise ratio. Secondly, extended scanning durations can cause discomfort for patients and increase the likelihood of motion artifacts.

Manuscript received March 1, 2024; revised July 28, 2024.

This work was supported in part by Hunan Provincial Natural Science Foundation of China (2023JJ50081and 2024JJ7268), and partly by the Scientific Research Fund of Hunan Provincial Education Department 20A273 and 22C0601.

Zhijun Luo, PhD, is an associate professor of the School of Mathematics and Finance, Hunan University of Humanities, Science and Technology, Loudi 417000, China (corresponding author to provide phone: 151-0738-0322; e-mail: ldlzj123@163.com).

Lirong Wang is a lecturer of the School of Mathematics and Finance, Hunan University of Humanities, Science and Technology, Loudi 417000, China (e-mail: ldwlr1234@163.com).

Zhibin Zhu is a Professor in the School of Mathematics and Computing Science, the Guangxi Colleges and Universities Key Laboratory of Data Analysis and Computation, Guilin University of Electronic Technology, Guilin 541004, China (e-mail: optimization_zhu@163.com).

Yingying Li is a teaching assistant of the School of Mathematics and Finance, Hunan University of Humanities, Science and Technology, Loudi 417000, China (e-mail:yingyli@qq.com).

Consequently, numerous researchers have focused on reducing acquisition time and improving imaging quality since the inception of MRI technology. One such approach is multi-coil parallel magnetic resonance imaging technology [2-3]. Nonetheless, inadequate spatial sampling violates the conventional Nyquist criterion, producing aliasing artifacts during the inverse Fourier transform process. To address this issue, the compressive sensing theory [4-5] proposes that accurate image reconstruction can be achieved from undersampled Fourier data, also known as k-space. Therefore, magnetic resonance imaging research based on compressive sensing theory has received widespread attention [6].

In dynamic magnetic resonance imaging research based on compressive sensing, the dynamic MRI reconstruction model can generally be expressed as

$$\min_X \frac{1}{2}\|\mathrm{A}X - B\|_F^2 + \alpha S(X), \tag{1}$$

where $\|\bullet\|_F$ represents the Fourier norm, $\|A\|_F^2 = \sqrt{tr(A^H A)}$, A^H denotes the Hermitian transpose of the matrix A, $X(m\times n\times d)$ is a dynamic MR image. d represents a dynamic image with d dynamics, each of which is the spatial dimension $m\times n$. The matrix $A = RF$ is the sampling operator, where R and F are the Fourier transform and sampling mask for each time frame, respectively. B represents undersampled data, $S(X)$ represents a sparse transformation, and α is the balance parameter. Based on the sparse representation theory, a series of methods for processing dynamic magnetic resonance reconstruction have been proposed successively, such as $k-t$ Sparse [7], $k-t$ Focus [3]. Its characteristic is that it does not use wavelet transform, does not directly enforce the sparsity of the image, but further sparses the image using initial estimated values [8]. Dynamic MRI data is correlated in both time and space, and the reconstruction results generated by such methods may be affected by low spatial or temporal resolution. For example, *k-t* Sparse performs well on cardiac MRI with periodic motion data but poorly on non-periodic data [9].

Recently, another popular strategy is to consider low rank in the model to find a solution that is both sparse and low rank (i.e., spatiotemporal MRI signals) [10]. This model type is known as the k-t SLR (*k-t* Sparse and Low-rank approach) model [11-12], which transforms a dynamic MR image into a so-called Casorati matrix, where each column and row correspond to a frame and a voxel, respectively. It can recover lost or damaged matrix terms under low-rank and incoherent conditions, further accelerating dynamic MRI. However, TV regularization in *k-t* SLR can reduce the efficiency of

reconstructed images due to the staircase effect. In recent years, some researchers have viewed dynamic MR images as a combination of low-rank components (L) and sparse components (S) and regularized them using different constraints to obtain the L+S model [13]. The main feature of this type of method is that by subtracting the background from the image, the remaining part becomes "sparser" than the dynamic image itself, which also brings broader application prospects for models based on compressive sensing.

Tr émoulh éac proposed the kt-RPCA model [1] by introducing robust principal component analysis (RPCA) [14-15], which uses the time Fourier transform of sparse components to reconstruct dynamic MRI as the sum of low-rank and sparse components. Compared with the reconstruction model regularized only by low-rank or sparse constraints, combining low-rank and sparse constraints can significantly improve dynamic imaging results. Due to its excellent performance, it has received attention and application since its proposal [16-21]. Yao et al. [22-23] summarized the dynamic MRI reconstruction model in such situations as:

$$\min_X \frac{1}{2}\|AX-B\|_F^2+\alpha\|X\|_*+\beta\|X\|_{TV} \tag{2}$$

where $\|\bullet\|_*$ represents the nuclear norm, which is the convex envelope of the rank function, $\|\bullet\|_{\mathrm{TV}}$ represents the total variation (TV) norm, α and β are parameters. Therefore, model (2) is a convex relaxation model that can be numerically solved using convex optimization algorithms, such as ADMM, primal-dual methods, etc. However, since incoherence may not always be satisfied in actual data, the optimal solution of traditional RPCA convex models may experience serious deviation [24]. In addition, in each iteration, the kernel norm requires a singular value decomposition of the matrix, which results in significant computation. Simply summing does not take into account the difference in singular value size. Finding alternatives to the kernel norm has become a new direction in research. In recent years, nonconvex penalty functions have successfully replaced the l_0-norm [25-26]. Inspired by this, researchers have introduced nonconvex methods into the study of magnetic resonance imaging, resulting in a series of meaningful achievements [27-29].

This article considers introducing the nonconvex minimax-concave (MC) penalty function into the model (2),

$$\min_X \frac{1}{2}\|AX-B\|_F^2+\alpha\phi_{MC}(X,a)+\beta\|X\|_{TV}.$$

We are constructing the new dynamic MRI reconstruction nonconvex model and decomposing the model using the primal-dual idea.

The rest of the paper is organized as follows: In Section 2, a new nonconvex model is constructed using the MC penalty function. The algorithm for solving this model is presented in Section 3; The experiment is given in Section 4. Finally, a summary is provided.

II. MCTV MODEL

In this section, we first review the definition and properties of the MC penalty function, then use this function to construct a regularization term and provide a dynamic MRI nonconvex model.

A. Minimax-concave (MC) penalty function

Definition 2.1. [25] The Minimax-concave (MC) penalty function $\phi_{MC}:\mathbf{R}\to\mathbf{R}$ is defined as

$$\phi_{MC}(x,a)=\begin{cases}|x|-\dfrac{a}{2}x^2, & |x|\le\dfrac{1}{a},\\ \dfrac{1}{2a}, & |x|>\dfrac{1}{a},\end{cases} \tag{4}$$

where $a>0$ is a parameter. Figure.1. shows the graph of parameters a with values of 0.5, 1, and 1.5, respectively.

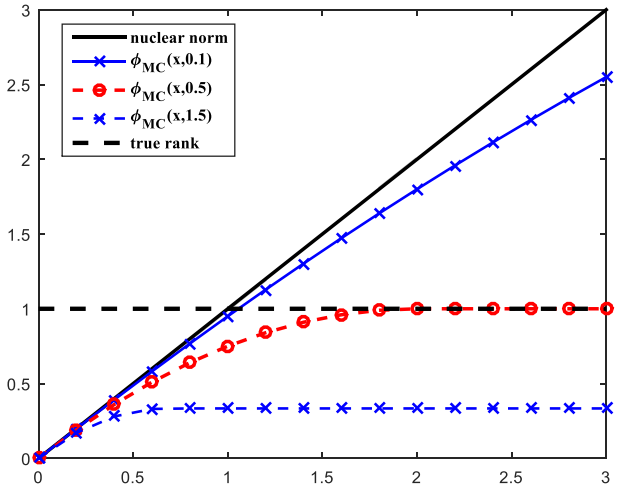

Fig. 1. $\phi_{MC}(x,a)$ penalty function

Inspired by the definition and graphics of the MC function, construct the following function $\psi_{MC}(x,a)$

$$\psi_{MC}(x,a)=|x|-\phi_{MC}(x,a), \tag{5}$$

as illustrated in Figure. 2.

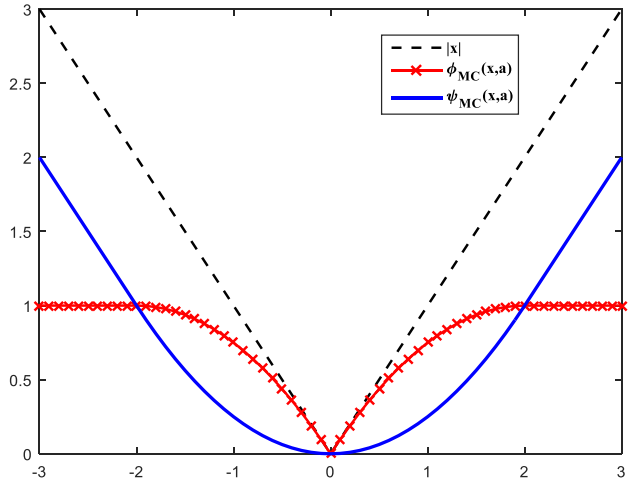

Fig. 2. $\psi_{MC}(x,a)$ function

From the definitions and graphs of functions $\phi_{MC}(x,a)$ and $\psi_{MC}(x,a)$, it can be inferred that functions $\phi_{MC}(x,a)$ and $\psi_{MC}(x,a)$ have the following properties.

Properties 2.1.

1) The function $\phi_{MC}(x,a)$ is a continuous nonconvex function, $\psi_{MC}(x,a)$ is a continuous convex function;

2) $\phi_{MC}(-x,a)=\phi_{MC}(x,a), \psi_{MC}(-x,a)=\psi_{MC}(x,a)$;

3) $0<\psi_{MC}(x,a)<|x|$;

4) If the parameter satisfies $0<a<1/\lambda$, then the function

$$\theta(x)=\lambda\phi_{MC}(x,a)+\frac{1}{2}(x-t)^2$$

is strictly convex, where λ is the parameter.

Proximity operators are essential in handling sparse models and regularization optimization problems [30]-[35]. Promoting sparsity enables models to achieve better interpretability and lower computational costs while maintaining predictive performance. Based on the definition and properties of the $\phi_{MC}(x,a)$ function, this article adopts the expression of

$$\phi_{MC}(x,a)=|x|-\psi_{MC}(x,a), \tag{6}$$

and its corresponding proximity operator is described as

$$\text{prox}_{\phi}(t;\lambda,a)=\arg\min_{x}\left\{\lambda\phi_{MC}(x,a)+\frac{1}{2}(x-t)^2\right\}, \tag{7}$$

where $\lambda>0$ is called the proximity parameter.

B. MCTV model

Figure 1 shows the $\phi_{MC}(x,a)$ function is more flexible in fitting performance than the kernel norm and has good penalty function properties. In the DMRI reconstruction model (2), we consider replacing the kernel norm with the MC function

$$\min_{X}\frac{1}{2}\|AX-B\|_F^2+\alpha\phi_{MC}(X,a)+\beta\|X\|_{TV}, \tag{8}$$

where $\phi_{MC}(\bullet)$ is a multivariate extension of (6), $\alpha\geq 0$, $\beta\geq 0$ is the regularization parameter.

To solve the model (8), firstly, we use the dual form of $\|X\|_{TV}$ as follows

$$\|X\|_{TV}=\max_{Y\in\Omega}\langle DX,Y\rangle_{\Omega}=\max_{Y\in\Omega}\langle -X,D\bullet Y\rangle_{X}, \tag{9}$$

where $\Omega=X\times X$, $Y\in\{\Omega:|Y|\leq 1\}$, D and $D\bullet$ represent gradient and divergence operators, respectively. The model (8) can be transformed into a min-max problem using the aforementioned dual formula (9),

$$\min_{X}\max_{Y\in\Omega}E(X,Y)=\frac{1}{2}\|AX-B\|_F^2+\alpha\phi_{MC}(X;a)-\beta\langle X,D\bullet Y\rangle_{X}. \tag{10}$$

If $\alpha=0$, $\beta>0$, then problem (10) is a total variational regularization model. If $\alpha>0$, $\beta=0$, then problem (10) is an MC function minimization model. Therefore, we refer to model (10) as the MCTV model.

III. ALGORITHM

In this section, we design a specific method for solving the problem(10). To simplify the expression, let

$$f(X)=\frac{1}{2}\|AX-B\|_F^2,$$

then the model be expressed as

$$\min_{X}\max_{Y\in\Omega}E(X,Y)=f(X)+\alpha\phi_{MC}(X;a)-\beta\langle X,D\bullet Y\rangle_{X}, \tag{11}$$

which is a typical min-max problem. The commonly used methods for solving such issues include ADMM [36], splitting algorithm[37], primal-dual algorithm[38], etc. This article uses the primal-dual and proximity-splitting framework to solve the problem (10), specifically,

$$\begin{cases} X_{k+1}=\arg\min_{X}\alpha\phi_{MC}(X,a)+\langle\nabla f(X_k),X-X_k\rangle-\beta\langle X,D\bullet Y_{k+1}\rangle \\ \qquad\qquad +\frac{1}{2\theta}\|X-X_k\|_F^2, \\ Y_{k+1}=\arg\min_{Y\in\Omega}\beta\langle(2X_{k+1}-X_k),D\bullet Y\rangle+\frac{1}{2\mu}\|Y-Y_k\|_F^2, \end{cases} \tag{12}$$

where, $\nabla f(X_k)=A^H(AX_k-B)$, $\alpha\geq 0,\beta\geq 0,\theta\geq 0,\mu\geq 0$ are parameters. Next, we discuss calculating the X and Y sub-problems separately.

For the X subproblem, after relaxing and omitting constants, it degenerates into the calculation of neighboring operators for the MC penalty function, i.e

$$X_{k+1}=\arg\min_{X}\frac{1}{2}\|X-X_k\|_F^2+\alpha\theta\phi_{MC}(X,a), \tag{13}$$

where $X_k=X_k-\theta(\nabla f(X_k)-\beta D\bullet Y_{k+1})$. Therefore, the problem (13) can be solved by referring to equation (7) to obtain the result.

The Y subproblem can be directly calculated using the gradient projection algorithm. Set $Y_k=Y_k+\beta\mu D(2X_{k+1}-X_k)$, then,

$$Y_{k+1}=\text{sgn}(Y_k)\cdot\min(|Y_k|,1), \tag{14}$$

where $\text{sgn}(\bullet)$ represents the sign function.

Now, we provide a specific algorithm, abbreviated as MCTV.

Algorithm (MCTV):
Step 0 Initialization:
Input matrices $A=RF$, B, given parameters $a>0$, $\alpha,\beta,\theta,\mu,\varepsilon$ and given initial values X_0,Y_0. Let k:=0;

Step 1: Compute X_{k+1} by (13);

Step 2: Compute Y_{k+1} by (14);

Step 3: Let $W_{k+1}=(X_{k+1},Y_{k+1})$, if $\|W_{k+1}-W_k\|^2\leq\varepsilon$, **STOP**; Otherwise, let $k:=k+1$ go back to **Step 1**.

IV. NUMERICAL EXPERIMENTS

This section conducts numerical experiments on the MCTV method proposed in the previous section to verify its effectiveness. The experimental data were obtained using the cardiac cine (cine 256*256*24) and cardiac infusion (perfusion 192*192* 40) provided in reference [22], as shown in the first line of Figure 3. Three common sampling types are selected for the sampling template, as shown in the second

row of Figure 4. They are Random, Cartesian, and Radial sampling templates from left to right. The testing environment for the heart movie experiment is 12GB of memory, 3.7GHz, MATLAB version R2018a.

The experiment is divided into two parts. In the first part, the cine data is reconstructed and compared with ktSLR [12], ktRPCA [1], and TVLR [22] in dynamic magnetic resonance studies. The second part conducts experiments on fusion data, with the primary purpose of verifying the convergence performance of the method and comparing it with TVLR.

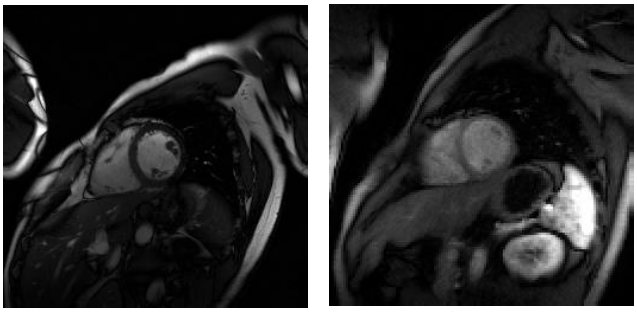

cine data perfusion data

Fig. 3. Experimental original data

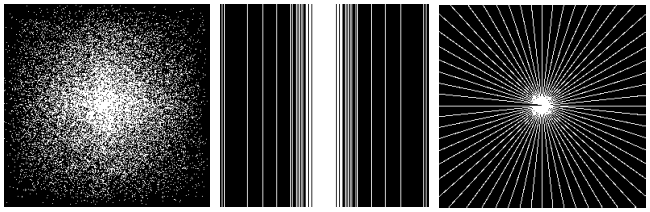

Fig. 4. Experimental sampling templates

In the experiment, the parameter settings provided in the literature were used. In the MCTV method proposed in this chapter, the MC penalty parameter a=0.05 was used, while the other parameters were set using the settings in TVLR [22].

The evaluation indicators include PSNR (Peak Signal-to-Noise Ratio), RMSE (Root Mean Squared Error), and CPU time, where PSNR is defined as follows:

$$\mathrm{PSNR} = 10\lg_{10}\frac{\left\|\mathrm{X}_{\mathrm{k}}\right\|_F^2}{\left\|\mathrm{X}_{\mathrm{k}} - X\right\|_F^2}.$$

A. Cine Data Testing

This subsection tests and compares the Cine data with some existing classical methods.

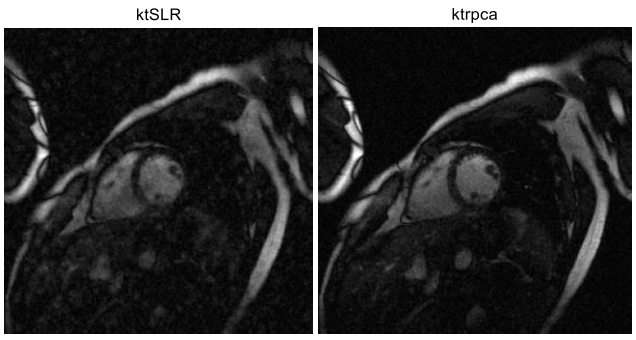

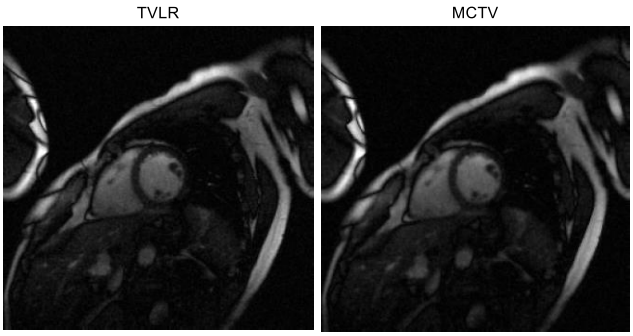

Fig. 5. Results under the Random template at 0.12 sampling rate

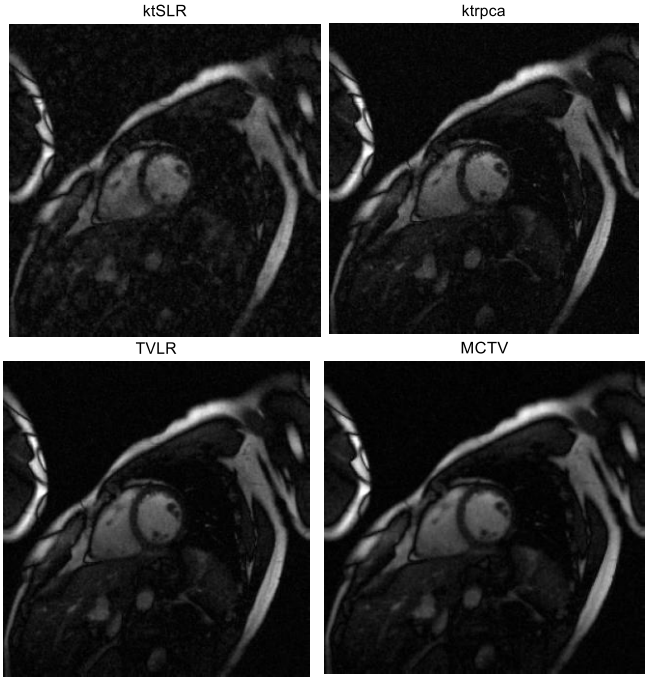

Fig. 6. Results under the Cartesia template at 0.18 sampling rate

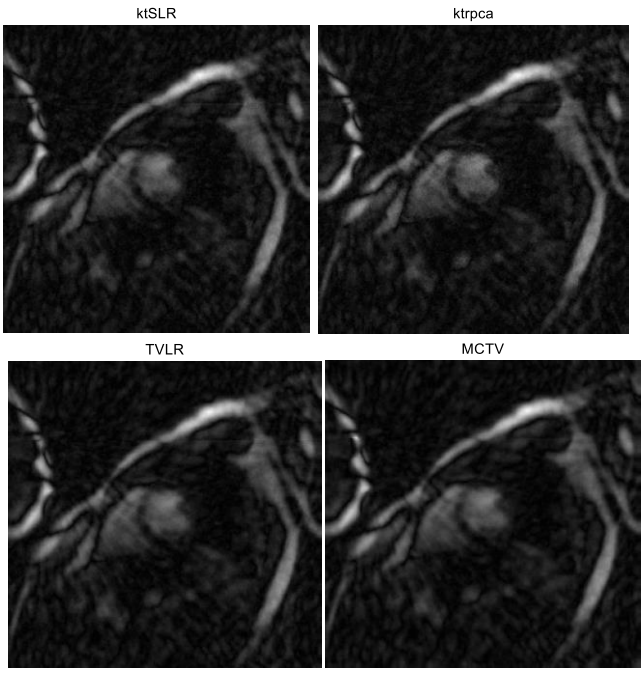

Fig. 7. Results under the radial template at 0.13 sampling rate

Figures 5-7 show the results of the 21st frame of the cine

sequence under various templates and methods. It can be seen from this that the reconstruction results of various methods vary under different sampling templates. The overall quality of reconstructed images obtained by the Random template with an intuitive upsampling rate of 0.12 is the best. In contrast, the quality of reconstructed images obtained by each method under the Radial template is poor. However, under different sampling templates, it can be seen that the reconstructed images obtained by the MCTV method perform the best among the four methods. Both ktSLR and ktRPCA have significant artifacts.

Figures 8-10 show the Boxplot of PSNR and RSME values obtained by four methods for data cine reconstruction under three different templates. The blue box represents the range of values that are relatively concentrated in the iteration, and the red line represents the mean. From this, it can be intuitively seen that the MCTV method proposed in this article has significant advantages under different sampling templates.

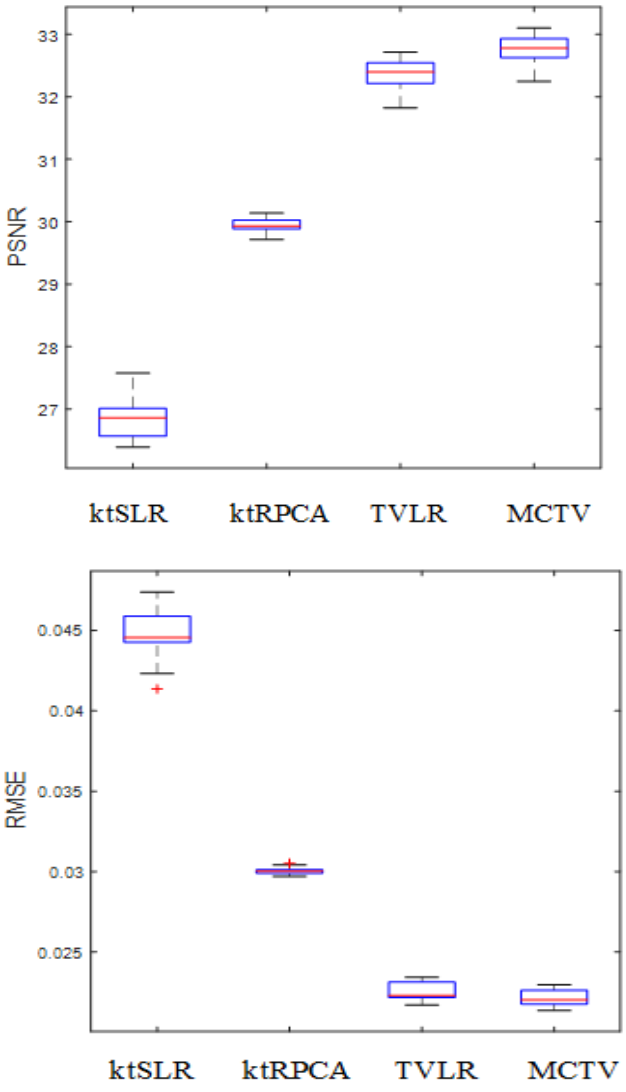

Fig. 8. Boxplot of PSNR and RMSE results under Random templates

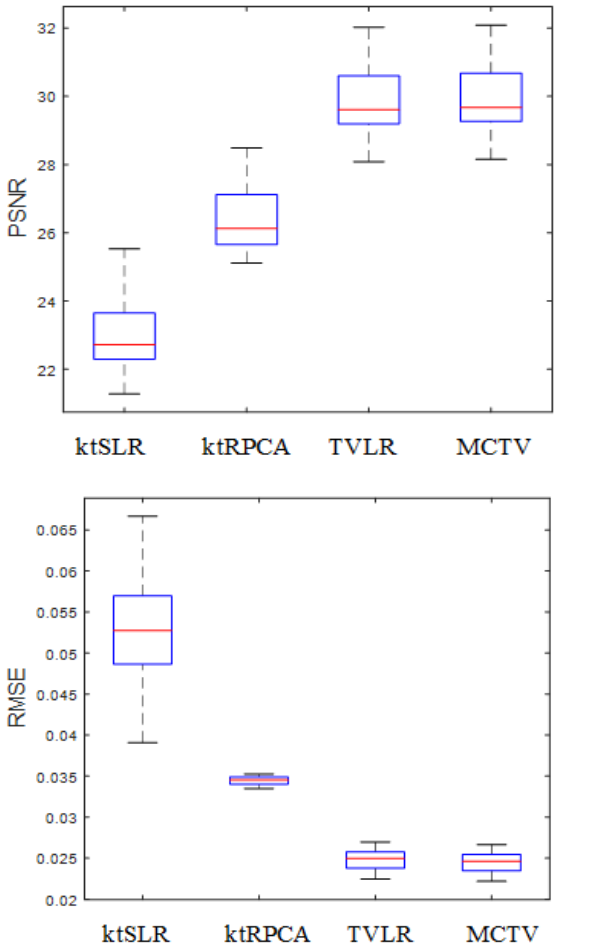

Fig. 9. Boxplot of PSNR and RMSE results under Cartesian templates

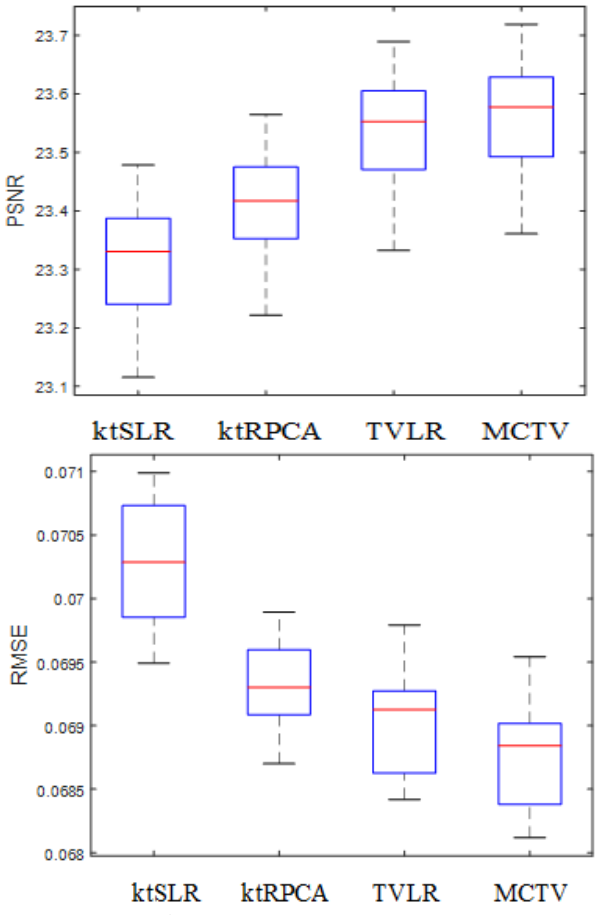

Fig. 10. Boxplot of PSNR and RMSE results under Radial templates

Scanning time is one of the most critical indicators in magnetic resonance imaging research. Table 1 shows the CPU time of each method, and it can also be seen that the MCTV method has a certain time advantage, while the ktSLR and ktRPCA methods take relatively longer.

TABLE I
CPU time comparison during the cine data reconstruction process

Data	Sampling Templates	Method	CPU Time/s
Cine	Random (0.12)	ktSLR	698
		ktRPCA	652
		TVLR	106
		MCTV	**96**
	Cartesian (0.18)	ktSLR	833
		ktRPCA	503
		TVLR	102
		MCTV	**93**
	Radial (0.13)	ktSLR	833
		ktRPCA	564
		TVLR	124
		MCTV	**106**

B. Perfusion Data Testin

This subsection applies the MCTV method proposed in this article to perfusion data to test the method's performance further. In the comparison in the previous section, we found that the ktSLR and ktRPCA methods are not as good as the TVLR method in terms of performance and have higher runtime costs. Therefore, this subsection is only comparable to the TVLR method.

Similar to the previous subsection, we conducted reconstruction tests on fusion data under three sampling templates. Firstly, we consider the numerical results of the reconstruction of the two methods when the residual RE is limited to 10^{-4}. We analyze them separately from the number of iterations, time, and generated PSNR values. The experimental results are shown in Table II, which shows that in the Radial sampling mode, the two methods have the most iterations and time consumption, and the PSNR value is relatively the smallest, which is similar to the results of the cine data.

TABLE II
Perfusion data limited residual RE=10^{-4} reconstruction numerical results

Templates	Method	Iterations	CPU time/s	PSNR/dB
Random	TVLR	70	97	32.52
	MCTV	**54**	**70**	**33.11**
Cartesian	TVLR	99	132	32.03
	MCTV	**84**	**110**	**32.64**
Radial	TVLR	236	306	29.57
	MCTV	**215**	**279**	**29.60**

Next, we will explore the convergence performance of the two methods. Figures 11-12 show the convergence curves of the two methods from the perspectives of iteration times and CPU running time, respectively. From the graph, it can be seen that both methods have good convergence. Under the same number of iterations (CPU time), the MCTV method proposed in this chapter has more obvious convergence.

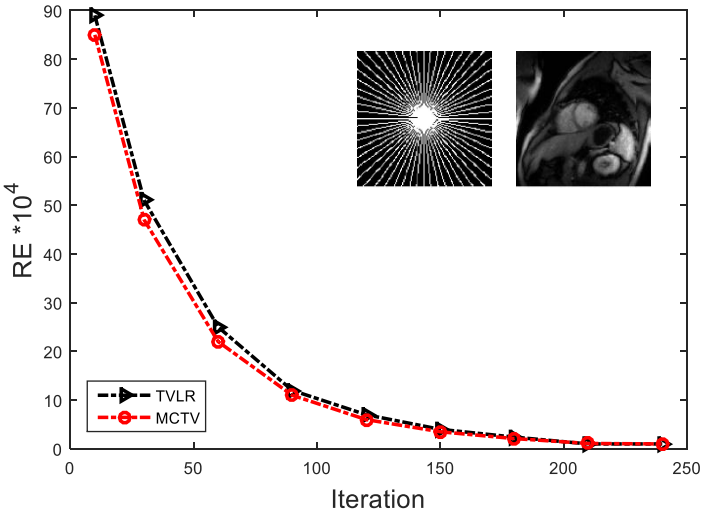

Figure. 11: Convergence curve under radial sampling

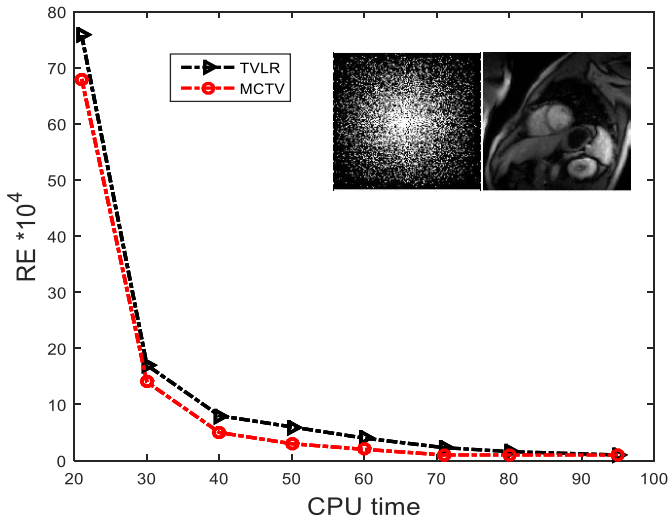

Figure. 12: Convergence curve under Random sampling

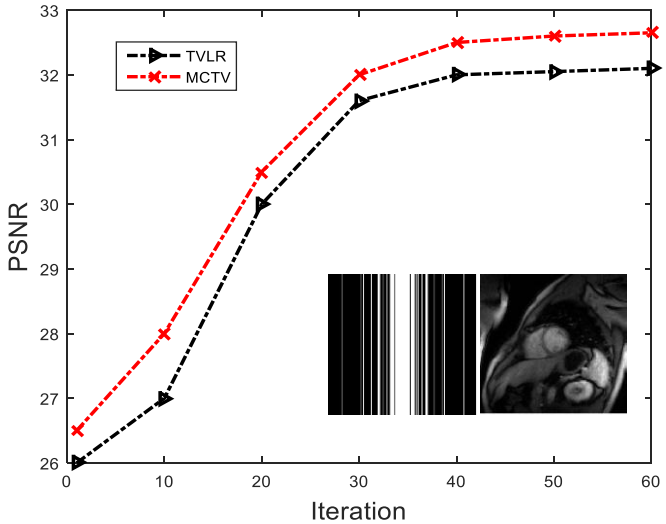

Figure. 13: Cartesian sampling iteration times and PSNR curve graph

V. Conclusion

A new nonconvex model is obtained by introducing the MC penalty function instead of the kernel norm in the dynamic magnetic resonance imaging model. In solving the model, a specific algorithm is constructed using the dual form of total variation and the proximity splitting framework. Numerical experiments show that the new method has good performance. The work that will be carried out next is to improve the new process and apply it to other medical imaging fields.

Acknowledgment

The authors would like to thank Prof. Ivan Selesnick (http://eeweb.poly.edu/iselesni/index.html) and Junfeng Yang (https://math.nju.edu.cn/jfyang) for sharing the Datas, MATLAB codes, and free download from their homepages.

References

[1] B. Trémoulhéac, N. Dikaios,"Dynamic MR image reconstruction separation from undersampled (k-t)-space via low-rank plus sparse prior," *IEEE Transactions on Medical Imaging*, vol. 33, no.8, pp1689-1701, 2014.

[2] H. Jung, J. C. Ye, and E. Y. Kim, "Improved k–t blast and k–t sense using focus," *Physics in Medicine & Biology*, vol. 52, no.11, pp3201, 2007.

[3] L. Feng, M. B. Srichai, and R. P. Lim, "Highly accelerated real-time cardiac cine MRI using k–t sparse-sense," *Magnetic Resonance in Medicine*, vol. 70, no.1, pp64-74, 2013.

[4] D. L. Donoho, "Compressed sensing," *IEEE Transactions on Information Theory*, vol. 52, no.4, pp1289-1306, 2006.

[5] E. J. Candes, J. Romberg, T. Tao, "Robust uncertainty principles: exact signal reconstruction from highly incomplete frequency information," *IEEE Transactions on Information Theory*, vol. 52, no.2, pp489-509, 2006.

[6] M. Lustig, D. L. Donoho, J. M. Santos, "Compressed Sensing MRI," *IEEE Signal Processing Magazine*, vol. 25, no.2, pp72-82, 2008.

[7] M. Lustig, J. M. Santos, D. L. Donoho, and J. M. Pauly. "Kt sparse: high frame rate dynamic MRI exploiting spatiotemporal sparsity." In Proceedings of the 13th annual meeting of ISMRM, Seattle, vol. 2420. 2006.

[8] J. C. Ye, "Compressed sensing MRI: a review from signal processing perspective." *BMC Biomedical Engineering*, vol. 1, no. 1, pp1-17, 2019.

[9] D. Wang, D. S. Smith, and X. Yang, "Dynamic MR image reconstruction based on total generalized variation and low-rank decomposition." *Magnetic Resonance in Medicine*, vol. 83, no.6, pp2064-2076, 2020.

[10] N. Vaswani, W. Lu, "Modified-CS: Modifying compressive sensing for problems with partially known support," *IEEE Transactions on Signal Processing*, vol. 58, no.9, pp4595-4607, 2010.

[11] S. G. Lingala, H. Yue, D. Edward, and J. Mathews, "Accelerated dynamic MRI exploiting sparsity and low-rank structure: kt SLR," *IEEE Transactions on Medical Imaging*, vol. 30, no. 5, pp1042-1054, 2011.

[12] S. G. Lingala, E. DiBella, G. Adluru, C. McGann, and M. Jacob, "Accelerating free-breathing myocardial perfusion MRI using multi-coil radial k− t SLR," *Physics in Medicine & Biology*, vol. 58, no.20, pp7309, 2013.

[13] R. Otazo, C. Emmanuel, and D. K. Sodickson, "Low-rank plus sparse matrix decomposition for accelerated dynamic MRI with separation of background and dynamic components," *Magnetic Resonance in Medicine*, vol. 73, no.3, pp1125-1136, 2015.

[14] E. J. Candès, X. Li, Y. Ma, and J. Wright, "Robust principal component analysis," *Journal of the ACM (JACM)*, vol. 58, no.3, pp1-37, 2011.

[15] X. Yuan, J. Yang, "Sparse and low-rank matrix decomposition via alternating direction methods," *Pacific J. Optim.*, vol. 9, no.1, pp167-180, 2013.

[16] T. M. Quan, T. Nguyen-Duc, W. K. Jeong, "Compressed sensing MRI reconstruction using a generative adversarial network with a cyclic loss," *IEEE Transactions on Medical Imaging*, vol. 37, no.6, pp1488-1497, 2018.

[17] Y. Zhang, P. T. Yap, G. Chen, W. Lin, L. Wang, and D. Shen, "Super-resolution reconstruction of neonatal brain magnetic resonance images via residual structured sparse representation," *Medical Image Analysis*, vol. 55, pp76-87, 2019.

[18] A. I. Aviles-Rivero, N. Debroux, G. Williams, M. J. Graves, and C. B. Schönlieb, "Compressed sensing plus motion (CS+M): a new perspective for improving undersampled MR image reconstruction," *Medical Image Analysis*, vol. 68, pp101933, 2021.

[19] S. Ma, J. Ai, H. Du, F. Fang, and W. Mei, "Recovering low-rank tensor from limited coefficients in any ortho-normal basis using tensor-singular value decomposition," *IET Signal Processing*, vol. 15, no.3, pp162-181, 2021.

[20] Z. He, Y. N. Zhu, S. Qiu, T. Wang, C. Zhang, B. Sun, X. Zhang, and Y. Feng, "Low-rank and framelet based sparsity decomposition for interventional MRI reconstruction, "*IEEE Transactions on Biomedical Engineering*, vol. 69, no.7, pp 2294-2304, 2022.

[21] H. Krishna, and R. Sharma, "Improving Orchestration Service Using gRPC API and P4-Enabled SDN Switch in Cloud Computing Platform: An OpenStack Case," *IAENG International Journal of Computer Science*, vol. 50, no.3, pp1083-1097, 2023.

[22] J. Yao, Z. Xu, X. Huang, and J. Huang, "An efficient algorithm for dynamic MRI using low-rank and total variation regularizations," *Medical Image Analysis*, vol. 44, pp14-27, 2018.

[23] Z. Zhu, J. Yao, Z. Xu, J. Huang, and B. Zhang, "A simple primal-dual algorithm for nuclear norm and total variation regularization," *Neurocomputing*, vol. 289, pp1-12, 2018.

[24] Z. Kang, C. Peng, and Q. Cheng, "Robust PCA via nonconvex rank approximation," 2015 IEEE International Conference on Data Mining. IEEE, pp211-220, 2015.

[25] I. Selesnick, A. Lanza, S. Morigi, and F. Sgallari, "Non-convex total variation regularization for convex denoising of signals," *Journal of Mathematical Imaging and Vision*, vol. 62, no.14, pp1-17, 2020.

[26] M. Doneva, "Mathematical models for magnetic resonance imaging reconstruction: An overview of the approaches, problems, and future research areas." *IEEE Signal Processing Magazine*, vol. 37, no.1, pp24-32, 2020.

[27] Y. Hu, X. Liu, M. Jacob, "A generalized structured low-rank matrix completion algorithm for MR image recovery," *IEEE Transactions on Medical Imaging*, vol. 38, no.8, pp1841-1851, 2018.

[28] M. Jacob, M. P. Mani, J. C. Ye, "Structured low-rank algorithms: Theory, magnetic resonance applications, and links to machine learning," *IEEE Signal Processing Magazine*, vol. 37, no.1, pp54-68, 2020.

[29] M. Qureshi, O. Inam, S. A. Qazi, I. Aslam, and H. Omer, "Tangent vector-based gradient method with l12-regularization: Iterative half thresholding algorithm for CS-MRI," *Journal of Magnetic Resonance*, vol. 333, pp107080, 2021.

[30] P. L. Combettes, J. C. Pesquet, "Proximal thresholding algorithm for minimization over orthonormal bases," *SIAM Journal on Optimization*, vol. 18, no.4, pp1351-76, 2008.

[31] N. Parikh, S. Boyd, "Proximal algorithms,"*Foundations and trends ® in Optimization*, vol. 1, no.3, pp127-239, 2014.

[32] Y. Tian, Y. Zhang, "A comprehensive survey on regularization strategies in machine learning," *Information Fusion*, vol. 80, pp146-166, 2020.

[33] J. Liu, B. Qiao, Y. Wang, W. He, and X. Chen, "Non-convex sparse regularization via convex optimization for impact force identification," *Mechanical Systems and Signal Processing*, vol. 191, pp110191, 2023.

[34] L.R. Wang, S. M. Deni, and Z. Zahid, "A LogTV Nonconvex Regularization Model for Magnetic Resonance Imaging," *Engineering Letters*, vol. 31, no.2, pp702-711, 2023.

[35] J. He, Y. M. Liu, and W. Lv, "A Modified Generalized Relaxed Splitting Preconditioner for Generalized Saddle Point Problems," *IAENG International Journal of Computer Science*, vol. 50, no.1, pp282-286, 2023.

[36] Y. Wang, W. Yin, J. Zeng, "Global convergence of ADMM in nonconvex nonsmooth optimization," Journal of Scientific Computing, vol. 78, pp29-63, 2019.

[37] P. L. Combettes, J. C. Pesquet, "Proximal splitting methods in signal processing," *Fixed-point Algorithms for Inverse Problems in Science and Engineering*, vol. 2011, pp185-212, 2011.

[38] A. Chambolle, T. Pock, "A first-order primal-dual algorithm for convex problems with applications to imaging," *Journal of Mathematical Imaging and Vision*, vol.40, pp120-145, 2011.